SERBIAN JOURNAL OF ELECTRICAL ENGINEERING
Vol. 18, No. 2, June 2021, 155-170
UDC: 004.932:[004.8:007.52 **DOI: https://doi.org/10.2298/SJEE2102155D**

Application of Metaheuristic Optimization Algorithms for Image Registration in Mobile Robot Visual Control

Lazar Đokić[1], Aleksandar Jokić[1], Milica Petrović[1], Nikola Slavković[1], Zoran Miljković[1]

Abstract: Visual Servoing (VS) of a mobile robot requires advanced digital image processing, and one of the techniques especially fitting for this complex task is Image Registration (IR). In general, IR involves the geometrical alignment of images, and it can be viewed as an optimization problem. Therefore, we propose Metaheuristic Optimization Algorithms (MOA) for IR in VS of a mobile robot. The comprehensive comparison study of three state-of-the-art MOA, namely the Slime Mould Algorithm (SMA), Harris Hawks Optimizer (HHO), and Whale Optimization Algorithm (WOA) is presented. The previously mentioned MOA used for IR are evaluated on 12 pairs of stereo images obtained by a mobile robot stereo vision system in a laboratory model of a manufacturing environment. The MATLAB software package is used for the implementation of the considered optimization algorithms. Acquired experimental results show that SMA outperforms HHO and WOA, while all three algorithms perform satisfactory alignment of images captured from various mobile robot poses.

Keywords: Visual Servoing, Mobile robot, Image registration, Whale optimization algorithm, Slime mould algorithm, Harris hawks optimizer.

1 Introduction

Visual servoing (VS) directly implies the usage of computer vision data acquired from a camera mounted on a robot to achieve optimal motion control of a mobile robot [1]. Therefore, a Mobile Robot (MR) can directly control its movement based on the camera motion and the vision data acquired from images obtained by cameras. In MR visual control, the error between the target and the current image is continuously measured. This error is used as a feedback signal for motion control to produce the required movement until the error reaches zero or a predefined error threshold. Feedback control and continuous measurements

[1]University of Belgrade, Faculty of Mechanical Engineering, Department of Production Engineering, Kraljice Marije 16, 11120 Belgrade, Serbia;
E-mails: ldjokic@mas.bg.ac.rs; ajokic@mas.bg.ac.rs; mmpetrovic@mas.bg.ac.rs; nslavkovic@mas.bg.ac.rs; zmiljkovic@mas.bg.ac.rs.

provide excellent robustness to errors in the system [2]. The image Registration (IR) function in VS of a MR is to extract useful information from images, such as geometric feature extraction, object classification, pattern recognition, etc. Time-consuming and computationally demanding methods for feature extraction can be mitigated with the utilization of direct methods that exploit pixel intensities [3]. Direct methods for visual control do not require metric information of the object, its shape, or camera motion, and they produce more robustness to the error. In direct VS, the pure image signal is used to design the vision-based control law and IR is utilized for the recovery of unknown parameters directly from measurable image quantities at each pixel in the image [4]. Therefore, intensity-based IR can be used to construct control error from the projective parameters that geometrically relate the current image with the target one [5]. For both IR and VS, two different images are compared. The first one is referred to as a target (fixed) image, while the other is referred to as the current (moving) image. This similarity allows for the seamless implementation of IR techniques in VS as proposed in [3] and [5]. In the previous papers, direct VS is recognized as the approach that utilizes IR for image processing. IR is a process of geometrical alignment of two images (the target and current image) and represents a crucial step in image preparation for the seamless execution of VS. In its nature, IR problem can be considered as an optimization problem with an aim to evaluate optimal Transformation Matrix (TM) elements to maximize image overlapping. There are various optimization approaches for IR, and in this paper, we propose the application of Metaheuristic Optimization Algorithms (MOA). One of the most common applications of MOA for IR is in medical imagery for combining nuclear magnetic resonance data and computer tomography [6]. Several successful applications of nature-inspired MOA can be found in [7] and [8], where particle swarm optimization [9] and genetic algorithms are used in multimodal medical IR. The implementation of the biologically inspired optimization methods showed superior exploration of the search space, better image alignment accuracy, and greater convergence speed compared to some of the traditional IR methods. Similar to the work proposed in this paper, research conducted in [10] suggests the implementation of particle swarm optimization, genetic algorithms, and grey wolf optimizer [11] for intensity-based IR in VS. However, we propose the utilization of different MOA, namely the Slime Mould Algorithm (SMA) [12], Harris Hawks Optimizer (HHO) [13], and Whale Optimization Algorithm (WOA) [14]. SMA showed satisfactory performance compared to the state-of-the-art MOA when used for solving classical engineering structural problems [12]. The simplicity of SMA allows for many modifications to be made in order to enhance the efficiency of the algorithm. Therefore, modified versions already have successful implementation for solving different digital image processing problems, such as the multilevel thresholding of multispectral images [15] and image segmentation of chest X-ray

images [16]. Likewise, HHO also finds an effective application in multilevel thresholding of color images [17] and image segmentation [18]. As one of the most established MOA, WOA have been successfully applied for solving various optimization problems in engineering [19]. Some of the notable applications of WOA are for task scheduling (e.g., MR scheduling [20]), image processing (e.g., multilevel image thresholding [21], and segmentation in magnetic resonance imaging [22]), etc.

An analysis of the three above-mentioned MOA algorithms (SMA, HHO, and WOA) for IR application is conducted in this work. All visual information of images obtained at different viewpoints during the motion of intelligent MR are analyzed. Target images are taken at the fixed MR pose (i.e., position and orientation), and both current and target images are acquired by two industrial-grade cameras (acA1920-25uc – Basler ace area scan cameras with Fujinon DF6HA-1B lenses). Camera and lens specification is given in **Table 1** and **Table 2,** respectively. Stereo image pairs are obtained by the stereo vision system of intelligent MR RAICO (Robot with Artificial Intelligence based COgnition) in the laboratory model of the manufacturing environment (Fig. 1). RAICO was developed at the Faculty of Mechanical Engineering in Belgrade within the Laboratory for Industrial Robotics and Artificial Intelligence (ROBOTICS & AI).

Table 1
The Basler acA1920-25uc camera specification.

Camera sensor / type of sensor	Sensor size [mm]	Resolution [px]	Pixel size [μm]	Frame rate [fps]
ON Semiconductor MT9P031 / CMOS	4.2 × 2.4	1920 × 1080	2.2 × 2.2	26

Table 2
The FUJINON DF6HA-1B lens specification.

Focal length [mm]	Aperture	Angle of view (Horizontal × Vertical) [˚]
6	f/1.4 – f16	57.3 × 43.8

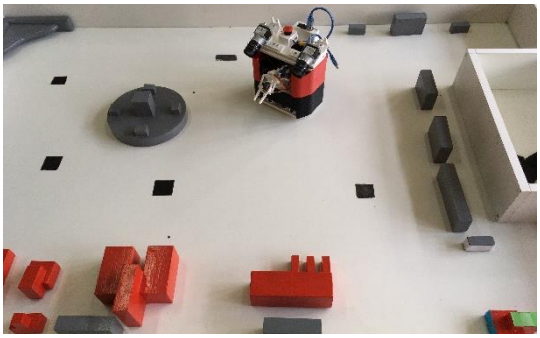

Fig. 1 – *Mobile robot RAICO in the laboratory model of the manufacturing environment.*

The paper is organized as follows. Section II describes the problem of intensity-based IR. In Section III, a short description of utilized optimization algorithms is provided. The mathematical formulation of Fitness Function (FF) is presented in Section IV. The results comparison of considered MOA for IR is presented in Section V while Section VI contains concluding remarks.

2 Intensity-based Image Registration

Intensity-based IR in VS is used to geometrically relate two images of the same manufacturing entity captured from different MR poses. First, MR is positioned in the desired pose, and target images are taken, while current images are taken at different camera viewpoints during the movement of MR. Current, as well as target images, must contain the same manufacturing entity to carry out intensity-based IR successfully. In addition, acquired images are preprocessed, that is, converted from RGB to binary images before IR is performed. Therefore, two binary images (target and current) of manufacturing entities are geometrically aligned. Target images before and after preprocessing can be seen in Fig. 2.

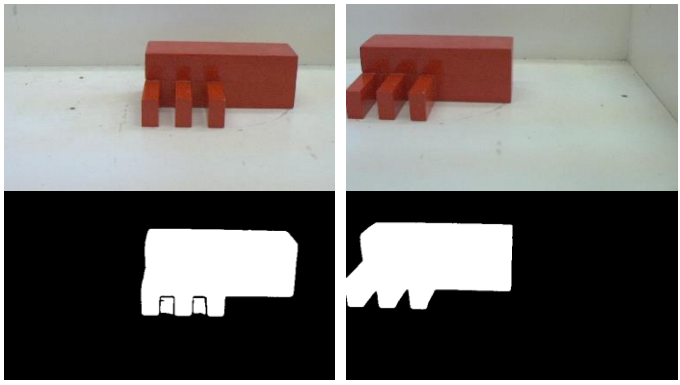

(a) (b)

Fig. 2 – (a) *Left and* (b) *right target image before and after preprocessing.*

Target images are converted to binary before motion initialization of MR, and current images are converted during motion of MR. The most computationally demanding part of image processing, in this case, is the implementation of MOA for IR. Due to this, real-time implementation of IR in VS of a mobile robot is still not realized. Therefore, MR movement is sequential, and the appropriate moving sequence depends on the ratio of translational velocities evaluated in each sequence. In [23], a similar vision-based control strategy is proposed and implemented for MR motion control. The objective of IR is to determine optimal spatial Transformation Matrix (TM) that best matches two images:

$$\boldsymbol{T} = \begin{bmatrix} s_X \cos(\theta) & -s_X \sin(\theta) & t_X \\ s_Y \sin(\theta) & s_Y \cos(\theta) & t_Y \\ 0 & 0 & 1 \end{bmatrix}, \tag{1}$$

where s_X and s_Y are scaling parameters with respect to x and y-axis, θ is the angle of image rotation, while t_X and t_Y represent translation along x and y-axis, respectively. The dimensions of the TM are 3×3, and optimal values of TM elements for geometrical alignment of two rigid bodies (manufacturing entities) are acquired via optimization algorithms.

3 Metaheuristic Optimization Algorithms

MOA have a wide application for solving assorted engineering problems. Compared to the deterministic optimization methods, they are considered computationally efficient with better solution exploration. However, there is no guarantee that the optimal solution will be found, and the performance of different MOA when solving the same problem does not guarantee the same solution. Based on the No Free Lunch (NFL) theorem for optimization [24], there is not any MOA with the best performance across all possible problems. Hence, to find the optimal problem solution, different MOA should be considered for different optimization tasks.

A brief description of the analyzed optimization algorithms for IR in VS are provided below.

3.1 Slime mould algorithm (SMA)

SMA is a metaheuristic algorithm that simulates the intelligent behavior of slime mould *Physarum polycephalum* while searching for food. The proposed algorithm utilizes adaptive weights for producing positive and negative feedback to find the optimal path to food (i.e., best solution). There are three different stages of SMA: (i) finding food ($rand \geq z$); (ii) approaching food ($r < p$); and (iii) wrapping food ($r \geq p$). In the first stage, searching for food is based on random distribution, and parameter z is used to define the threshold between the exploration and exploitation phase of SMA. Slime mould approaching behavior is determined by the concentration of food odor in the air, and wrapping simulates slime mould venous tissue contraction. The location of slime mould while approaching and wrapping food is updated by:

$$\boldsymbol{X}(t+1) = \begin{cases} r\left(\boldsymbol{Ub} - \boldsymbol{Lb}\right) + \boldsymbol{Lb}, & r < z, \\ \boldsymbol{X}_b(t) + \boldsymbol{v}_b\left(\boldsymbol{WX}_A(t) - \boldsymbol{X}_B(t)\right), & r < p, \\ \boldsymbol{v}_c \boldsymbol{X}(t), & r \geq p, \end{cases} \tag{2}$$

where $\boldsymbol{X}$ is the location of slime mould, t represents the current iteration of the algorithm, $\boldsymbol{X}_b$ is the location with the highest odor concentration, $\boldsymbol{X}_A$ and $\boldsymbol{X}_B$ are randomly selected individuals from the population, $\boldsymbol{Lb}$ and $\boldsymbol{Ub}$ are the lower and upper bounds of the search range, and r is a random number in the range [0 1]. p is calculated with:

$$p = \tanh\left|S(i) - DF\right|, \tag{3}$$

where $S(i)$ represents the fitness value of $\boldsymbol{X}$, and DF is the best-obtained fitness value of all iterations. Values of the parameter $\boldsymbol{v}_b$ are within the following range represented with:

$$\boldsymbol{v}_b = \left[-\operatorname{arctanh}\left(-\frac{t}{\max(t)}+1\right), \operatorname{arctanh}\left(-\frac{t}{\max(t)}+1\right)\right], \tag{4}$$

and values of $\boldsymbol{v}_c$ are in the range [–1 1]. The mathematical formulation of adaptive weight $\boldsymbol{W}$ is given by:

$$\boldsymbol{W}\left(SmellIndex(i)\right) = \begin{cases} 1 + r\log\left(\dfrac{bF - S(i)}{bF - wF}+1\right), & i \le \dfrac{\mathrm{N}}{2}, \\ 1 - r\log\left(\dfrac{bF - S(i)}{bF - wF}+1\right), & i > \dfrac{\mathrm{N}}{2}, \end{cases} \tag{5}$$

$$SmellIndex = sort(S), \tag{6}$$

where bF and wF represent the best and worst obtained fitness value in the current iteration, and N is the number of individuals in the population. Parameters $\boldsymbol{v}_b$, $\boldsymbol{v}_c$, and $\boldsymbol{W}$ are utilized for the variation of slime mould venous tissue width during foraging. The satisfactory performance of SMA is mainly contributed to the ability to maintain the balance between exploration and exploitation [12].

3.2 Harris hawks optimizer (HHO)

HHO is a biologically based technique of artificial intelligence, inspired by the cooperative behavior of Harris's hawks during the hunt. As well as other metaheuristic optimization algorithms, HHO has two main searching steps, exploration ($|E| \ge 1$) and exploitation ($|E| < 1$). The transition between these two steps is determined based on the energy of prey defined in (7):

$$E = 2E_0\left(1 - \frac{t}{\mathrm{T}}\right), \tag{7}$$

where E is escaping energy of the prey, E_0 is the initial energy, t is the current iteration, and T is the total number of iterations. During the exploration phase ($|E| \ge 1$) of HHO, hawks' position is evaluated by:

$$\boldsymbol{X}(t+1)=\begin{cases}\boldsymbol{X}_{rand}(t)-r_1\left|\boldsymbol{X}_{rand}(t)-2r_2\boldsymbol{X}(t)\right|, & q\geq 0.5,\\ \left(\boldsymbol{X}_{prey}(t)-\boldsymbol{X}_{m}(t)\right)-r_3\left(\boldsymbol{Lb}+r_4\left(\boldsymbol{Ub}-\boldsymbol{Lb}\right)\right), & q<0.5,\end{cases} \tag{8}$$

where vector $\boldsymbol{X}(t+1)$ defines the position of hawks in the following iteration t, $\boldsymbol{X}(t)$ is the current position vector of hawks, $\boldsymbol{X}_{prey}(t)$ is the current position of prey, $\boldsymbol{X}_{rand}(t)$ represents one randomly selected hawk, $\boldsymbol{X}_{m}$ is the value of the average position of hawks in the current population, r_1, r_2, r_3, r_4, and q are random values within range [0 1]. $\boldsymbol{Lb}$ and $\boldsymbol{Ub}$ are the lower and upper bounds of the searched variables.

In the exploitation phase ($|E| < 1$) of the algorithm, four strategies are implemented based on the various chasing styles of hawks and escaping actions of the prey: (i) soft besiege ($r \geq 0.5$ and $|E| \geq 0.5$); (ii) soft besiege with progressive rapid dives ($r < 0.5$ and $|E| \geq 0.5$); (iii) hard besiege ($r \geq 0.5$ and $|E| < 0.5$); (iv) hard besiege with progressive rapid dives ($r < 0.5$ and $|E| < 0.5$). The aforementioned strategies implemented in the exploitation phase of HHO utilize different mathematical models for updating position vector $\boldsymbol{X}(t+1)$. For more information about the mathematical formulation of strategies used in the exploitation phase, the reader is referred to [13]. Different searching strategies based on uniformly distributed random value r and dynamically randomized time-varying escaping energy of prey E greatly improve both exploration and exploitation properties of HHO while also allowing for a seamless transition between diversification and intensification.

3.2 The whale optimization algorithm (WOA)

The WOA is based on an intelligent hunting strategy utilized by humpback whales as they pursue fish schools. In the exploration phase of the algorithm, whales (agents) are searching and encircling their prey. This phase of WOA is mathematically formulated with:

$$\boldsymbol{X}(t+1)=\boldsymbol{X}_{rand}(t)-\boldsymbol{AD}, \tag{9}$$

$$\boldsymbol{D}=\left|\boldsymbol{C}.\boldsymbol{X}_{rand}(t)-\boldsymbol{X}(t)\right|, \tag{10}$$

$$\boldsymbol{A}=2\boldsymbol{ar}-\boldsymbol{a},\quad \boldsymbol{C}=2\boldsymbol{r}, \tag{11}$$

where t is the current iteration, $\boldsymbol{X}_{rand}$ represents the position vector of the randomly selected agent. In (10), element-wise multiplication is used, and it is denoted with the dot. Coefficient vector $\boldsymbol{A}$ can take value in the range [$-a$ a], while parameter a linearly decreases to zero through iterations and vector $\boldsymbol{r}$ takes random values within range [0 1].

After the exploration phase, the obtained solution should be in the vicinity of global optima, and the exploitation phase based on the bubble-net attacking method commences. This method includes a shrinking encircling mechanism and

a spiral update procedure simultaneously used by whales when they are approaching the prey. Based on the uniform distribution, an agent will update its location by using a shrinking encircling mechanism or a spiral update procedure (12):

$$\boldsymbol{X}(t+1)=\begin{cases}\boldsymbol{X}^{*}(t)-\boldsymbol{AD}, & p\geq 0.5,\\ \boldsymbol{D}'\mathrm{e}^{\mathrm{b}l}\cos(2\pi l)+\boldsymbol{X}^{*}(t), & p<0.5,\end{cases} \tag{12}$$

where p and l are random values within range [0 1] and [–1 1], respectively. b is a variable used to define a shape of a logarithmic spiral and $\boldsymbol{D}'$ represents the distance between the best-obtained solution and i-th whale, given in (13):

$$\boldsymbol{D}'=\left|\boldsymbol{X}^{*}(t)-\boldsymbol{X}(T)\right|, \tag{13}$$

where position vector $\boldsymbol{X}^{*}(t)$ represents the currently best-positioned agent so far.

The transition between the two phases of the algorithm is based on the value of vector coefficient $\boldsymbol{A}$. When $|\boldsymbol{A}|\geq 1$, the exploration phase of the algorithm is utilized and when $|\boldsymbol{A}|<1$, the exploitation phase occurs. As a result, there is a clear separation between these two phases which causes high local optima avoidance and effective problem solving with unknown search space [14].

4 Fitness Function

Fitness Function (FF) is used to provide an estimation of the geometrical alignment of the target and current stereo image pairs. A better geometrical alignment is obtained when FF has a lower value. Therefore, the optimization goal is to minimize the proposed FF. For evaluating FF, Sum of Squared Differences (SSD) for two images is used (14):

$$SSD(\boldsymbol{I}_1,\boldsymbol{I}_2)=\sum_{(u,v)\in\boldsymbol{I}}\left(\boldsymbol{I}_1[u,v]-\boldsymbol{I}_2[u,v]\right)^2, \tag{14}$$

where $\boldsymbol{I}_1$ is the target image, $\boldsymbol{I}_2$ is a spatially transformed current image, and u and v are pixel coordinates of given images. In order to match the current image with the target one, a spatial transformation of the current image is executed using TM. In the optimization process, a lower value of SSD for two images means better image overlapping and indicates that optimal design variables are evaluated. The elements of TM represent design variables (θ, s_X, s_Y, t_X, and t_Y), and their lower and upper bounds are defined with (15):

$$\begin{aligned}\boldsymbol{Lb}&=[-5,\ 0.7,\ 0.7,-20,-20],\\ \boldsymbol{Ub}&=[+5,\ 1.2,\ 1.2,\ 20,\ 20],\end{aligned} \tag{15}$$

where ***Lb*** and ***Ub*** represent the lower and upper bounds for θ, s_X, s_Y, t_X, and t_Y, respectively.

It can be concluded that an optimal solution is one with a minimal value of FF. Therefore, adequate velocities of MR can be computed based on optimally generated elements of TM.

5 Experimental Results

In this section, the performance of the Slime mould algorithm, the Harris hawks optimizer, and the Whale optimization algorithm are compared. Mentioned algorithms are described in Section III, and their implementation for IR in VS is analyzed in this section.

In **Table 3** are given 12 different posses with known displacements from the desired pose in which intelligent mobile robot RAICO was positioned. In each pose, two images (left and right image) are acquired with a stereo vision system. In total, 24 images (12 stereo image pairs) are used for testing of IR. The adopted coordinate system of MR RAICO can be seen in Fig. 3.

Table 3
Current pose displacements compared to the target pose.

Stereo image pairs	1	2	3	4	5	6	7	8	9	10	11	12
x [cm]	0	0	0	0	–4	–2	2	4	2	4	0	0
z [cm]	2	–2	–4	–6	0	0	0	0	–2	–4	0	0
θ [°]	0	0	0	0	0	0	0	0	0	0	5	–5

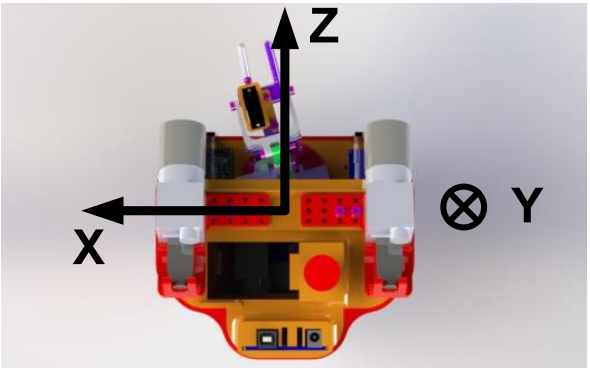

Fig. 3 – *The adopted coordinate system of mobile robot.*

5.1 Optimization parameters setting

MOA parameters have a significant effect on optimization results and parameter setting is necessary to properly implement optimization algorithms for IR. All three considered algorithms are population-based, and a number of agents (N), as well as a number of iterations (T) are selected for tuning. Furthermore, all considered MOA have two phases (exploration and exploitation), and in order to determine the optimal ratio between these phases, for each algorithm, appropriate parameters will be tuned. Various combinations of the above-mentioned parameters for each algorithm, as well as average (for 5 repetitions) and the best average FF values for all images can be seen in **Table 4**, **Table 5**, and **Table 6**.

Table 4

Average and the best average fitness function values of SMA.

N	T	avg / best avg	z = 0.03	z = 0.02	z = 0.01
50	50	avg	5369.17	5449.28	5451.73
		best avg	5314.92	5360.50	5353.46
	100	avg	5271.31	5257.00	5324.19
		best avg	5206.88	5185.79	5224.00
100	50	avg	5231.52	5255.89	5330.87
		best avg	5178.79	5204.21	5299.63
	100	avg	**5166.64**	5167.23	5202.30
		best avg	5154.17	**5125.00**	5126.21

Table 5

Average and the best average fitness function values of HHO.

N	T	avg / best avg	E = [3 0]	E = [2.5 0]	E = [2 0]
50	50	avg	7174.26	7162.18	7204.54
		best avg	7006.08	7030.5	6842.08
	100	avg	6860.38	6815.35	6748.1
		best avg	6642.38	6518.79	6531.54
100	50	avg	6577.12	6646.74	6675.93
		best avg	6324.29	6266.79	6461.17
	100	avg	6427.55	6280.42	**6231.51**
		best avg	5989.38	**5964.92**	5987.92

Table 6
Average and the best average fitness function values of WOA.

N	T	avg / best avg	a = [4 0]	a = [3 0]	a = [2 0]
50	50	avg	7006.87	7099.08	7037.83
		best avg	6828.42	7003.25	6804.92
	100	avg	6813.98	6865.96	6953.13
		best avg	6315.96	6546.79	6703.75
100	50	avg	6532.08	6627.21	6674.23
		best avg	6420.96	6167.58	6351.71
	100	avg	**6185.39**	6291.49	6443.13
		best avg	**5932.58**	6100.63	6233.92

All combinations of parameters are run 5 times and the total number of conducted tests is 180 (60 for each algorithm). The reported results are procured in MATLAB environment running on a workstation with AMD Ryzen 5 3600 3.6GHz (4.2GHz) processor and 16 GB of RAM.

The best average and average results for five repetitions of considered algorithms obtained in **Table 4**, **Table 5**, and **Table 6** suggest better algorithm performance when both the number of agents (N) and the number of iterations (T) is set to 100. Different ratios between exploration and exploitation of SMA, HHO, and WOA do not have a significant effect on algorithm performance. In **Table 4**, the best average result is obtained when parameter z is set to the default value of 0.02, and an average value of FF for five runs of the algorithm is just slightly worse than the best-recorded result of average FF value for five runs. It can be seen from **Table 5** that the ratio between exploration and exploitation again does not have any significant impact on algorithm performance. However, WOA performs better when the exploration phase of the algorithm is utilized more and records the best results when parameter a is set in the range [4 0].

The overall best results are recorded when SMA is implemented for IR, while HHO and WOA are outperformed by SMA and record similar results.

5.2 Comparison of the experimental results

For comparison of optimization algorithms, we consider cases in which the best average FF value is obtained. Acquired SSD values for left and right images of stereo pairs are shown in Figs. 4a and b, respectively.

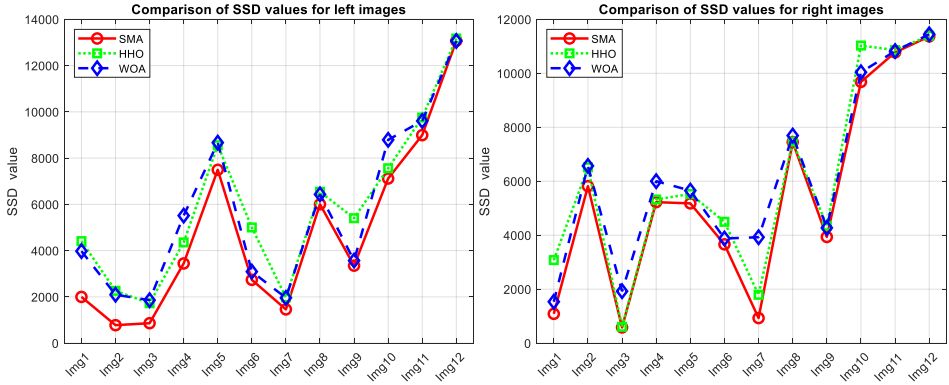

(a) (b)

Fig. 4 – *Comparison of SSD values for* (a) *left and* (b) *right images of stereo pairs.*

From Fig. 4, it is evident that SSD values have an increasing trend due to increased disparity between the current and target images. The lowest values of SSD are recorded when the third stereo image pair is geometrically aligned with target images. The highest values of SSD are registered for the eleventh and twelfth stereo pair due to the initial rotation of 5° and –5° about the *z*-axis, respectively. Experimental results from [10] also reported similar SSD values when genetic algorithms were implemented for IR. Moreover, obtained experimental results also note evaluation of different SSD values for corresponding left and right images of stereo pair. The higher difference between SSD values for images of the same stereo pair implies computing of different MR velocities. TM elements evaluated from geometrical alignment with lower SSD value should be considered relevant for MR velocities' computation.

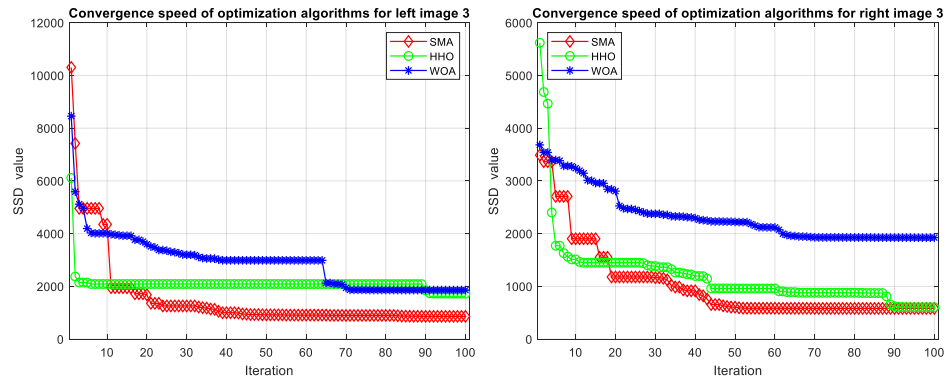

(a) (b)

Fig. 5 – *Comparison of algorithms convergence speed for* (a) *left and* (b) *right image of stereo pair 3.*

Fig. 5 shows the comparison of convergence speed of FF for the third stereo pair. The results presented in Fig. 5 show faster convergence of HHO. However, in both cases (both images), SMA outperforms HHO. In Fig. 5a, HHO and WOA reached a similar value of FF, while SMA reached a minimal FF value. In Fig. 5b, SMA and HHO reached a similar value of FF, with SMA reaching a slightly lower value, and WOA is outperformed by both algorithms.

Fig. 6 displays overlapping of the target images of stereo pair and current images of stereo pair 3.

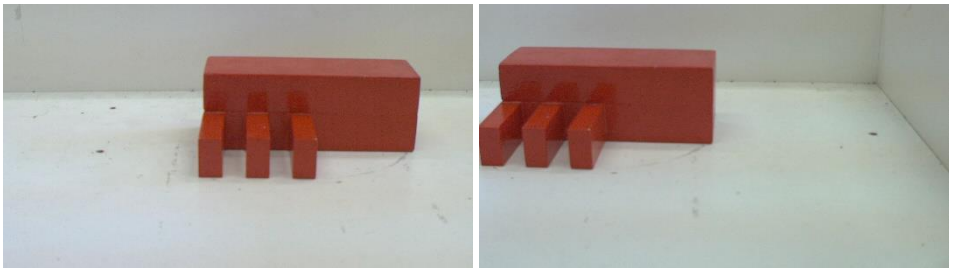

(a)

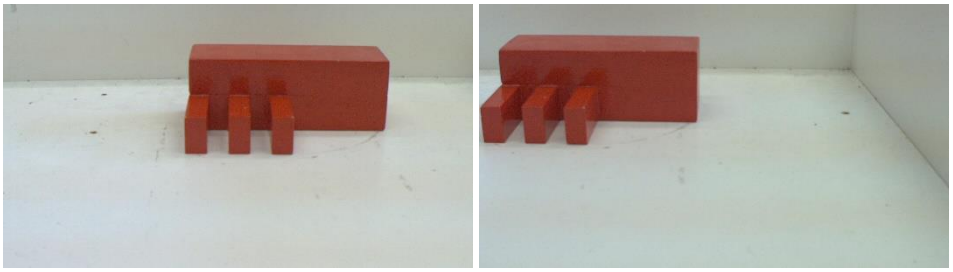

(b)

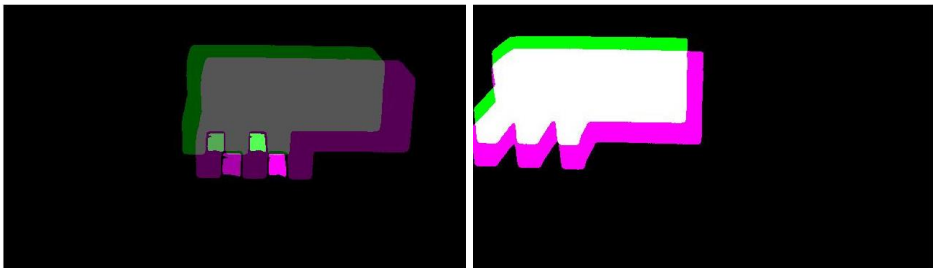

(c)

Fig. 6 – (a) *Left and right target images;* (b) *Left and right images of stereo pair 3;* (c) *Initial geometrical alignment.*

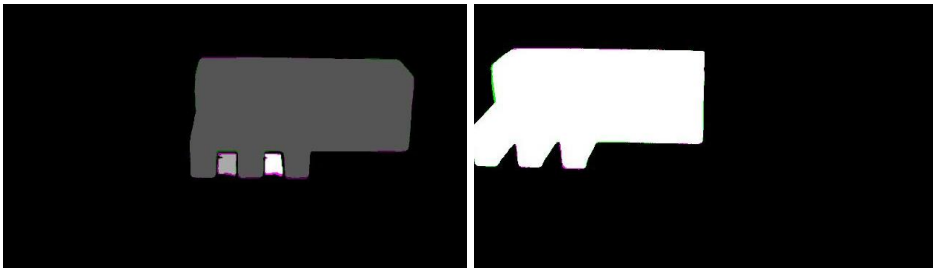

(a)

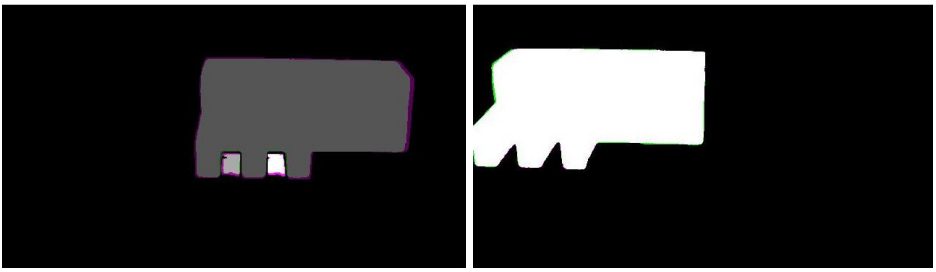

(b)

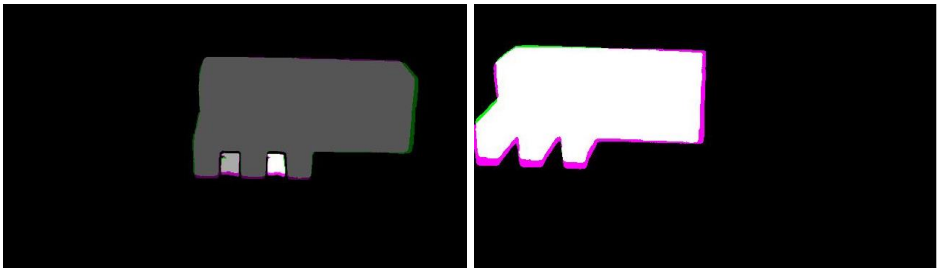

(c)

Fig. 7 – (a) *Geometrical alignment after implementation of SMA;*
(b) *Geometrical alignment after implementation of HHO;*
(c) *Geometrical alignment after implementation of WOA.*

Initial geometrical alignment and comparison of geometrical alignment of target images of stereo pair and current images of stereo pair 3 after implementation of SMA, HHO, and WOA can be seen in Fig. 7. Geometrical alignment of images of stereo pair 3 are represented since minimal FF value is reached. Consequently, evaluated TM elements used for spatial transformation of current images of stereo pair 3 almost perfectly overlap with target images after transformation. Overlapping of images is presented with gray and white color. On the contrary, green and pink colors are used to illustrate no overlapping of observed manufacturing entities. This can be best seen in Fig. 6c.

6 Conclusion

Applicability of different Metaheuristic Optimization Algorithms (MOA), i.e., Slime Mould Algorithm (SMA), Harris Hawks Optimizer (HHO), and Whale Optimization Algorithm (WOA) for Image Registration (IR) are evaluated on a set of 12 stereo image pairs. All images used for IR are acquired in a laboratory model of a manufacturing environment with a stereo vision system of the mobile robot RAICO. Based on the comparison of the experimental results, successful geometrical alignment of current and target images is possible for current images with minor initial displacements. Geometrical alignment of stereo image pairs with major initial displacements, where observed manufacturing entity is partially seen, were not successful. Therefore, the proposed methodology for IR in Visual Servoing (VS) can be primarily implemented for fine positioning of a mobile robot in the desired pose. Further work should be directed towards real-time implementation of IR in VS of a mobile robot while executing transportation and manipulation tasks, as well as towards the evaluation of new fitness functions relevant for such tasks.

7 Acknowledgment

This work has been financially supported by the Ministry of Education, Science and Technological Development of the Serbian Government, through the project "Integrated research in macro, micro, and nano mechanical engineering – Deep learning of intelligent manufacturing systems in production engineering", under the contract number 451-03-9/2021-14/200105, and by the Science Fund of the Republic of Serbia, grant number 6523109, AI-MISSION4.0, 2020-2022.

8 References

[1] F. Chaumette, S. Hutchinson, P. Corke: Visual Servoing, Ch. 34, Springer Handbook of Robotics, Edited by B. Siciliano, O. Khatib, Springer, Berlin, 2016.

[2] P. Corke: Robotics, Vision and Control: Fundamental Algorithms in MATLAB, 2nd Edition, Springer, Berlin, 2017.

[3] G. Silveira, E. Malis: Visual Servoing from Robust Direct Color Image Registration, Proceedings of the IEEE/RSJ International Conference on Intelligent Robots and Systems, St. Louis, MO, USA, October 2009, pp. 5450−5455.

[4] M. Irani, P. Anandan: About Direct Methods, Proceedings of the International Workshop on Vision Algorithms: Theory and Practice, Corfu, Greece, September 1999, pp. 267−277.

[5] G. Silveira, E. Malis: Direct Visual Servoing: Vision-Based Estimation and Control Using Only Nonmetric Information, IEEE Transactions on Robotics, Vol. 28, No. 4, August 2012, pp. 974−980.

[6] B. Zitova, J. Flusser: Image Registration Methods: A Survey, Image and Vision Computing, Vol. 21, No. 11, October 2003, pp. 977−1000.

[7] M.P. Wachowiak, R. Smolíková, Y. Zheng, J.M. Zurada, A.S. Elmaghraby: An Approach to Multimodal Biomedical Image Registration Utilizing Particle Swarm Optimization, IEEE Transactions on Evolutionary Computation, Vol. 8, No. 3, June 2004, pp. 289−301.

[8] F.L. Seixas, L.S. Ochi, A. Conci, D.M. Saade: Image Registration Using Genetic Algorithms, Proceedings of the 10th Annual Conference on Genetic and Evolutionary Computation, Atlanta, GA, USA, July 2008, pp. 1145−1146.

[9] J. Kennedy, R. Eberhart: Particle Swarm Optimization, Proceedings of the International Conference on Neural Networks (ICNN'95), Perth, WA, Australia, November 1995, pp. 1942−1948.

[10] L. Đokić, A. Jokić, M. Petrović, Z. Miljković: Biologically Inspired Optimization Methods for Image Registration in Visual Servoing of a Mobile Robot, Proceedings of the 7th International Conference on Electrical, Electronic and Computing Engineering (IcETRAN 2020), September 2020, pp. 715−720.

[11] S. Mirjalili, S.M. Mirjalili, A. Lewis: Grey Wolf Optimizer, Advances in Engineering Software, Vol. 69, March 2014, pp. 46−61.

[12] S. Li, H. Chen, M. Wang, A.A. Heidari, S. Mirjalili: Slime Mould Algorithm: A New Method for Stochastic Optimization, Future Generation Computer Systems, Vol. 111, October 2020, pp. 300−323.

[13] A.A. Heidari, S. Mirjalili, H. Faris, I. Aljarah, M. Mafarja, H. Chen: Harris Hawks Optimization: Algorithm and Applications, Future Generation Computer Systems, Vol. 97, August 2019, pp. 849−872.

[14] S. Mirjalili, A. Lewis: The Whale Optimization Algorithm, Advances in Engineering Software, Vol. 95, May 2016, pp. 51−67.

[15] M.K. Naik, R. Panda, A. Abraham: Normalized Square Difference Based Multilevel Thresholding Technique for Multispectral Images Using Leader Slime Mould Algorithm, Journal of King Saud University-Computer and Information Sciences, November 2020, pp. 1−13.

[16] M. Abdel-Basset, V. Chang, R. Mohamed: HSMA_WOA: A Hybrid Novel Slime Mould Algorithm with Whale Optimization Algorithm for Tackling the Image Segmentation Problem of Chest X-ray Images, Applied Soft Computing Journal, Vol. 95, October 2020, pp. 1−19.

[17] X. Bao, H. Jia, C. Lang: A Novel Hybrid Harris Hawks Optimization for Color Image Multilevel Thresholding Segmentation, IEEE Access, Vol. 7, June 2019, pp. 76529−76546.

[18] E. Rodriguez-Esparza, L.A. Zanella-Calzada, D. Oliva, A.A. Heidari, D. Zaldivar, M. Pérez-Cisneros, L.K. Foong: An Efficient Harris Hawks-Inspired Image Segmentation Method, Expert Systems with Applications, Vol. 155, October 2020, pp. 1−29.

[19] F.S. Gharehchopogh, H. Gholizadeh: A Comprehensive Survey: Whale Optimization Algorithm and Its Applications, Swarm and Evolutionary Computation, Vol. 48, August 2019, pp. 1−24.

[20] M. Petrović, Z. Miljković, A. Jokić: A Novel Methodology for Optimal Single Mobile Robot Scheduling Using Whale Optimization Algorithm, Applied Soft Computing Journal, Vol. 81, August 2019, pp. 1−25.

[21] S.J. Mousavirad, H. Ebrahimpour-Komleh: Multilevel Image Thresholding Using Entropy of Histogram and Recently Developed Population-Based Metaheuristic Algorithms, Evolutionary Intelligence, Vol. 10, No. 1-2, July 2017, pp. 45−75.

[22] A. Mostafa, A.E. Hassanien, M. Houseni, H. Hefny: Liver Segmentation in MRI Images based on Whale Optimization Algorithm, Multimedia Tools and Applications, Vol. 76, No. 23, December 2017, pp. 24931−24954.

[23] M. Petrović, A. Mystkowski, A. Jokić, L. Đokić, Z. Miljković: Deep Learning-Based Algorithm for Mobile Robot Control in Textureless Environment, Proceedings of the 15th International Conference Mechatronic Systems and Materials (MSM 2020), Bialystok, Poland, July 2020, pp. 1−4.

[24] D.H. Wolpert, W.G. Macready: No Free Lunch Theorems for Optimization, IEEE Transactions on Evolutionary Computation, Vol. 1, No. 1, April 1997, pp. 67−82.